European Journal of Agronomy 156 (2024) 127169

Contents lists available at ScienceDirect

European Journal of Agronomy

journal homepage: www.elsevier.com/locate/eja

Unraveling the spatial-temporal patterns of typhoon impacts on maize during the milk stage in Northeast China in 2020

Qiang Zhang [a,b,c], Geli Zhang [c], Xiangming Xiao [d], Yao Zhang [e], Nanshan You [a], Yuanyuan Di [a], Tong Yang [c], Yingli He [a], Jinwei Dong [a,b,*]

[a] Key Laboratory of Land Surface Pattern and Simulation, Institute of Geographic Sciences and Natural Resources Research, Chinese Academy of Sciences, Beijing, China
[b] University of Chinese Academy of Sciences, Beijing, China
[c] College of Land Science and Technology, China Agricultural University, Beijing, China
[d] School of Biological Sciences, Center for Earth Observation and Modeling, University of Oklahoma, Norman, OK, USA
[e] Sino-French Institute for Earth System Science, College of Urban and Environmental Sciences, Peking University, Beijing, China

ARTICLE INFO

Keywords:
Typhoon
Maize
Milk stage
LSWI
Spatial-temporal compensation
Google Earth Engine

ABSTRACT

Typhoons are increasing in inland areas and affecting agriculture under climate change. Assessing the large-scale impact of typhoons on crops is essential for improving agricultural resilience. However, typhoon impacts are typically intricate and uncertain, depending on the different stages of crop growth and the indicators used for assessment. Here, we leveraged satellite data to examine the spatial-temporal patterns of typhoon-induced impacts on maize during the milk stage in Northeast China in 2020. We found that land surface water index (LSWI) showed a significantly higher negative relative change of 161.5% in regions severely affected by typhoons, surpassing that of normalized difference vegetation index (NDVI, 19.7%), near-infrared reflectance of vegetation (NIR_V, 31.7%), and enhanced vegetation index (EVI, 25.2%), suggesting the outperformance of LSWI in monitoring the impact of typhoons on maize. Based on LSWI, we revealed the spatial-temporal distribution of typhoon impacts. Specifically, significant impacts on maize growth were observed in central Northeast China, particularly in Heilongjiang (49% of maize fields) and Jilin provinces (53% of maize fields). Furthermore, week-long lagging typhoon impacts on maize growth were generally found but lasted until the end of the maize growing season. We also found the typhoon impacts were partially mitigated by spatial and temporal compensations. Regions with above-average maize growth offset the losses experienced in areas severely affected by typhoons. Additionally, better maize growth in the early stages enhanced its resilience against subsequent typhoon impacts. Despite the mitigating effects on maize production, typhoons may increase the risk of maize mold, which warrants further investigation. Given the projected increase in future climate extremes, this study provides valuable insights into the rapid assessment of typhoon impacts using satellite data and cloud computing and supports decision-making in crop management for sustainable agricultural production.

1. Introduction

Typhoons, a kind of tropical cyclone occurring in the northwest Pacific, is one of the most dangerous and devastating extreme weather events (EWEs) (Needham et al., 2015), which have severe impacts on terrestrial ecosystems and human welfare (Patrick et al., 2022). They are usually accompanied by sustained high winds, intensive rainfall, high storm surges, and coastal inundation, and influence regional ecological and agricultural sustainability (Fan et al., 2021), such as reducing grain yield (Fischer and Stapper, 1987), increasing drying costs, decreasing grain quality, and slowing down harvest (Berry et al., 2004). Typhoons particularly affect taller crops such as maize. Lodging that occurs during the milk, dough, and dent stages may result in aborted kernels, reduced grain quality, and reduced kernel weight (Abendroth et al., 2011; Nleya et al., 2016). Even at the physiological maturity stage, lodging caused by natural disasters can lead to yield losses (Nleya et al., 2016). Recent studies indicated the frequency and intensity of cyclone activities would increase in higher latitudes in the coming decades in the context of

* Corresponding author at: Key Laboratory of Land Surface Pattern and Simulation, Institute of Geographic Sciences and Natural Resources Research, Chinese Academy of Sciences, Beijing, China.
E-mail address: dongjw@igsnrr.ac.cn (J. Dong).

https://doi.org/10.1016/j.eja.2024.127169
Received 15 August 2023; Received in revised form 17 March 2024; Accepted 19 March 2024
Available online 26 March 2024

irreversible global climate change (Elsner et al., 2008), which would further threaten terrestrial ecosystems and regional food security (Lesk et al., 2016).

The assessment of the impacts of typhoons has been traditionally based on field surveys and aerial photography (Kupfer et al., 2008; Wang and Xu, 2009), which can provide detailed information on vegetation damage along the track of typhoons (Imbert, 2018). However, field observation-based studies are often constrained to a local scale because they are time-consuming and expensive (Hoque et al., 2016). Remote sensing is a cost-effective technique for understanding typhoon impacts on vegetation at the regional scale (Smith et al., 2014). For example, the high temporal resolution of MODIS data makes it ideally suited for rapidly assessing typhoon disturbance, and it has frequently been used in the analyses of the impacts of typhoons and hurricanes on vegetation (de Beurs et al., 2019; Rossi et al., 2013).

Remote sensing-based assessments of typhoon impacts have shown limited attention to crops in previous studies, with a predominant on forests (Rossi et al., 2013; Wang et al., 2010; Zhang et al., 2013). Vegetation Indices (VIs) derived from satellite images have been widely used to examine the severity and extent of vegetation disturbances (Jing et al., 2014; Tortini et al., 2017), and the main VIs include normalized difference vegetation index (NDVI) (Abbas et al., 2020), enhanced vegetation index (EVI) (Wang and D'Sa, 2009), land surface water index (LSWI) (Zhou et al., 2017), and near-infrared reflectance (NIR_V) (Wang et al., 2020). NDVI, NIR_V, and EVI are both greenness-related VIs, and their disturbance detection is based on changes in chlorophyll content (Huete et al., 1994), which are the most frequently used indices for detecting vegetation disturbance under typhoons. Moreover, NIR_V, the product of total scene NIR reflectance (NIR_T) and the normalized NDVI, can estimate crop biomass accumulation of terrestrial vegetation and consistently untangles the confounding effects of background brightness, leaf area, and the distribution of photosynthetic capacity with depth in canopies (Badgley et al., 2017). It has been used for global and regional-scale crop biomass accumulation estimations (Badgley et al., 2019), crop growth monitoring (Wu et al., 2020), and natural disaster assessment (Smith et al., 2020). While, LSWI, a water-related vegetation index (Xiao et al., 2004), is more sensitive to the leaf water content and vegetation modifications (Anderson et al., 2004; Hardisky et al., 1983). It has proven to be a superior indicator to NDVI and EVI in assessing typhoon impacts in forests in previous studies (Gang et al., 2020; Wang et al., 2010). Previous research using the above VIs to study the influences of typhoons on vegetation is mostly focused on forests rather than crops (Tortini et al., 2017; Zhang et al., 2013). In terms of the impacts of EWEs on crops, most of the concerns are drought events (Wang et al., 2020; Wolf et al., 2016). The sensitivities of these different kinds of VIs to typhoon impacts on crops remain unclear, despite the risk of typhoons on crops increasing with global warming (Kossin et al., 2014).

Spatial patterns of disturbances are vital to assess the impacts of typhoons on vegetation. Previous studies showed significant correlations between the distance to the typhoons and forest structural loss at the regional scale as the wind speed decreases away from typhoons (Negrón-Juárez et al., 2014; Schwartz et al., 2017). Typhoon strength decreases as it moves inland, and decreases at a larger radius from the eyewall of the typhoon (Negrón-Juárez et al., 2014), which is also further modified by terrain (Philippopoulos and Deligiorgi, 2012). On the other hand, the temporal dynamics of disturbance on vegetation are also worthy of concern in assessing the impacts of EWEs. For instance, the warmer springs can alleviate the impacts of summer heatwave and drought on vegetative photosynthesis, resulting in no significant declines in crop biomass accumulation across most of Europe during the main vegetative growing season (Wang et al., 2020). Furthermore, the spatial and temporal impacts may work together on the final disturbance patterns of the impacts of EWEs on vegetation. Wolf et al. (2016) found that increased carbon uptake in the eastern United States during the warm spring of 2012 compensated for large reductions by the summer drought in the Midwest, which mitigated the impact on net annual carbon uptake. Therefore, the spatial-temporal patterns of disturbance are significant for understanding vegetation dynamics concerning typhoon influence on the entire region (Stanturf et al., 2007). Unfortunately, few studies focused on the overall spatial-temporal patterns of typhoon impacts on vegetation.

As an increasingly important grain bowl in China, Northeast China produces more than one-third of the maize production in China. Unfortunately, three typhoons (Bavi, Maysak, and Haishen) hit Northeast China (Table S1), covering most of the maize planting areas from August 27th to September 8th in 2020, which coincided with the maize milk stage (Figs. 1 and 2). The typhoon impacts on maize aggravates the uncertainty of food security in China created by the ongoing pandemic of coronavirus disease 2019 (COVID-19)—with breaks in food supply chains, food shortages, and food price spikes predicted (Ma et al., 2021). A timely, unbiased, and transparent assessment of the impacts of the three typhoons on maize is extremely important but still unavailable.

The objective of this study is to investigate the overall impacts of the three typhoons on maize growth and production in Northeast China in 2020 through the utilization of high precision maize map and four VIs (NDVI, EVI, NIR_V, and LSWI) as well as the cloud platform Google Earth Engine (GEE). Specifically, we aim to address the following questions: 1) Which proxy is more sensitive to typhoon impacts on maize? 2) How many maize fields in Northeast China were affected by typhoons, and what were the seasonal and spatial patterns of typhoon impacts? 3) Was maize yield largely impacted by typhoons in 2020? This study expects to provide an unbiased assessment of the typhoon impacts on maize in Northeast China in 2020 and develop a framework for future rapid monitoring of typhoon impacts on agricultural production.

2. Materials and methods

2.1. Study area

Northeast China includes three provinces (Heilongjiang, Jilin, and Liaoning) and four municipalities in eastern Inner Mongolia (hereafter referred to as eastern Inner Mongolia), covering a vast area of 1.2×10^6 km^2 (about 13% of China's territory). The region has a cold temperate and humid/sub-humid climate. The average annual precipitation is approximately 500–800 mm, which mostly falls in July and August. The annual accumulated air temperatures above 0 and 10 °C vary from 2000–4200 °C·day and 1600–3600 °C·day, respectively. The number of frost-free days varies between 140 d and 170 d. One crop per year is cultivated under such thermal conditions in this region. The impacts of typhoons in Northeast China have been largely overlooked due to their lower frequency than in tropical regions; however, the increasing frequency of typhoons in the context of climate change (Emanuel, 2005) and global wind speeds recovery in high latitudes (Zeng et al., 2019) are increasingly threatening regional food production and security.

2.2. Data

2.2.1. Spatial distribution and phenology of maize

We used the recent 10-m crop-type maps with an overall accuracy of 86% in Northeast China during 2017–2019 (You et al., 2021) as the base maps of our study region. This high-quality maize map can provide detailed information on maize while helping to filter out the distractions of other crops. We overlaid the three years of maize maps to generate the maize layer as our study region considering the impact of land use changes. We then resampled it to the 500-m spatial resolution to match the Moderate Resolution Imaging Spectroradiometer (MODIS) data (Fig. 1a). Fig. 1b showed that maize in Northeast China is mainly distributed in plain areas.

The maize phenology data is derived from the China Meteorological Science Data Center (CMSDC) (http://data.cma.cn/). The growth period of maize is from mid-May to early October in Northeast China (Fig. 2).

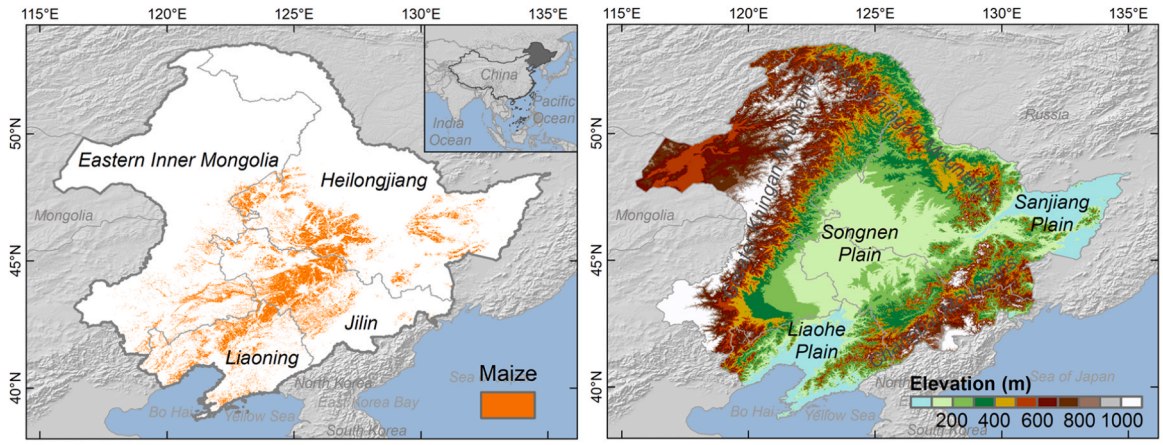

Fig. 1. The distribution of maize fields and topography in Northeast China.

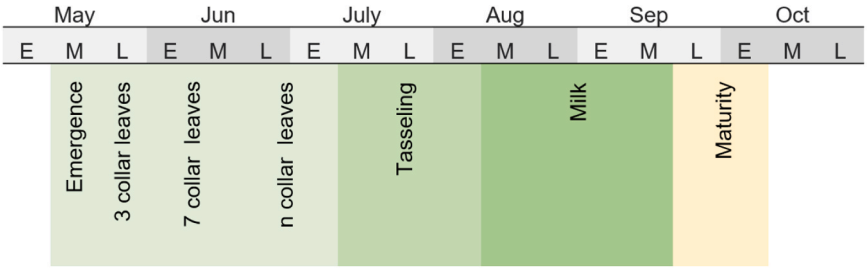

Fig. 2. The calendar of maize in Northeast China. The capital letters "E", "M", and "L" represent the first ten days, the middle ten days, and the third ten days of the month respectively.

When the three typhoons happened, the maize was going through the milk stage (Table S1, Fig. 2). During this period, maize would go through the milk, dough, and dent stages, which are all important periods for rapid accumulation of starch and nutrients (Abendroth et al., 2011; Nleya et al., 2016).

2.2.2. Satellite-based VIs from MODIS

We selected three kinds of spectral indices for assessing the disturbance of vegetation, including three greenness indices (NDVI, NIR_V, and EVI) (Abbas et al., 2020; Rossi et al., 2013), one water-related index (LSWI) (Zhou et al., 2017). The 500-m nadir bidirectional reflectance distribution function-adjusted reflectance (NBAR) dataset (MCD43A4.006) of MODIS was used to generate the time series of VIs, which has been proven to outperform others for vegetation dynamics monitoring (Li et al., 2018; Schaaf et al., 2002). Here we procured all accessible MCD43A4 Collection 6 NBAR data spanning the years 2017–2020. The maximum value composites were used to synthesize the data to the 8-day temporal resolution to mitigate the impacts of bad observations. All data processing was conducted in the GEE platform. NDVI, EVI, NIR_V, and LSWI were calculated by using the following formulas:

$$NDVI = \frac{\rho_{nir} - \rho_{red}}{\rho_{nir} + \rho_{red}} \quad (1)$$

$$EVI = G \cdot \frac{\rho_{nir} - \rho_{red}}{\rho_{nir} + C_1 \cdot \rho_{red} - C_2 \cdot \rho_{blue} + L} \quad (2)$$

$$NIR_V = \rho_{nir} \cdot NDVI \quad (3)$$

$$LSWI = \frac{\rho_{nir} - \rho_{swir}}{\rho_{nir} + \rho_{swir}} \quad (4)$$

where G, C_1, C_2, and L are coefficients for the MODIS EVI algorithm (G=2.5, C_1=6, C_2=7.5, and L=1), and ρ_{nir}, ρ_{red}, ρ_{blue}, and ρ_{swir} represent the surface reflectance for the near-infrared, red, blue, and shortwave-infrared bands, respectively.

2.2.3. Typhoon tracks and related meteorological data

We acquired the routes of the three typhoons to track the typhoons across Northeast China in 2020 from the Typhoon Network of the Central Meteorological Observatory (Fig. 3a). The three typhoons entered Northeast China on August 27th (day of year (DOY) 240), September 3rd (DOY 247), and September 8th (DOY 252), 2020, and stayed for 9 hours, 27 hours and 5 hours, respectively. We also used total precipitation and maximum wind speed data from the CMSDC to represent the meteorological anomalies caused by the three typhoons.

2.2.4. In-situ UAV survey during the typhoons

To timely understand the impacts of typhoons on maize, we observed five plots of maize near the typhoon tracks by the Unmanned Aerial Vehicle (UAV) from September 9th to September 15th, 2020 (after Typhoon Haishen) (Fig. 3a). The sample sites were selected from the five counties which have been reported with typhoons' impacts. The UAV images clearly show the distribution of maize lodging in these sites (Fig. 3), which could be regarded as the in-situ observation evidence for assessing typhoon impacts on maize.

2.2.5. Maize area and yield from National Bureau of Statistics

The maize area and yield data were collected from the National Bureau of Statistics (http://www.stats.gov.cn/), including the maize area and yield from 2017 to 2020 for each city in Northeast China.

2.3. Methods

The framework was developed for rapidly assessing the overall impacts of typhoons on maize growth and production (Fig. 4). We first

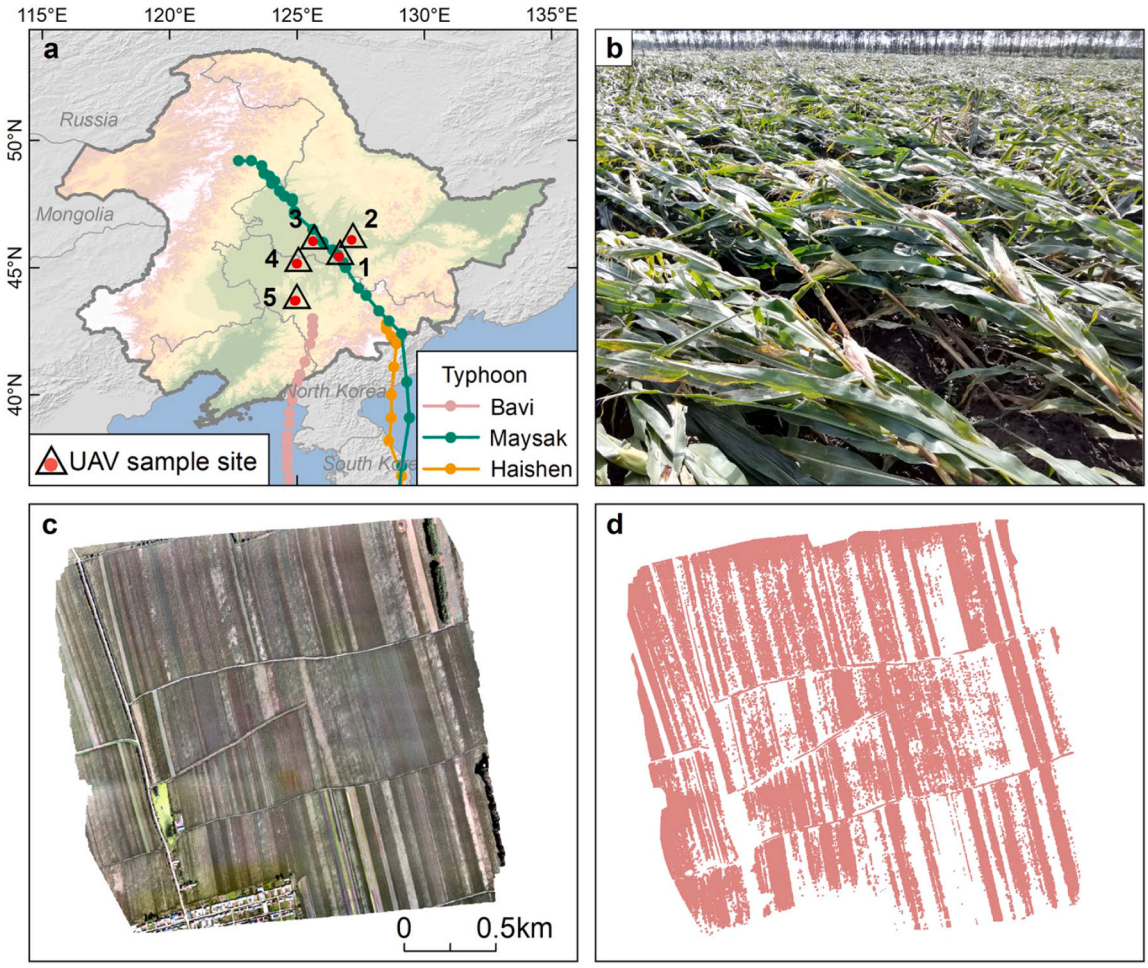

Fig. 3. The tracks of the three typhoons and the location of five UAV sample sites. (a) The relative position of the UAV sample sites and the typhoon routes. (b) The in-situ photographs of the landscape of site 1. (c) The original UAV composite image of site 1. (d) The affected maize areas of site 1. Other original UAV composite images and the corresponding affected areas can be referred to in Fig. S1.

compared the sensitivity of VIs at the site and the regional scales to obtain the prior indicator. Then we used it to quantify the maize fields that have been affected in Northeast China and verified with the meteorological anomalies caused by the typhoons. Finally, we analyzed the seasonal and spatial variations of maize disturbance from typhoons and tried to answer whether maize production has been primarily affected due to the typhoons in Northeast China in 2020.

2.3.1. Detecting the sensitivity of VIs to typhoon impacts on maize

Here we used the relative change of VIs (ΔVIs (%)) to indicate the sensitivity of different VIs to typhoon impacts on maize, which has been widely used to quantify vegetation disturbance (Peereman et al., 2020; Wang and Xu, 2018). The ΔVIs (%) with an 8-day temporal resolution for each pixel in 2020 were derived relative to the multiyear means from 2017–2019, as there were no EWEs in Northeast China during the three consecutive years (Fig. 5a,b). The ΔVIs (%) of the UAV sample sites and the entire study area were calculated by averaging the pixels. The calculation formulas are as follows:

$$VI_{Anomaly} = VI_{2020} - VI_{Baseline} \quad (5)$$

$$\Delta VIs(\%) = \frac{VI_{Anomaly}}{VI_{Baseline}} \quad (6)$$

where ΔVIs (%) represents the sensitivity of VIs to typhoon impacts. The $VI_{Anomaly}$ denotes the difference of VI (NDVI / EVI / NIR_V / LSWI) between 2020 and baseline (2017–2019). The VI_{2020} and $VI_{Baseline}$ refer to the VI value in 2020 and the mean VI value from 2017 to 2019, respectively. The higher absolute values of ΔVIs (%) mean higher sensitivity of one proxy to typhoon impacts.

2.3.2. Seasonal and spatial variations of typhoon impacts on maize

The impacts of typhoons on the development of maize at a seasonal scale should be considered, although the three typhoons occurred at the end of August and early September when the maize was growing during the milk stage in this region (Fig. 2, Table S1). The impacts of typhoons (e.g., lodging) may affect the crop biomass accumulation of maize. The NIR_V, which is highly correlated with crop biomass accumulation, has been used to analyze the spatial and temporal dynamics of vegetation growth (Badgley et al., 2019; Wang et al., 2021). Here, we first acquired the monthly NIR_V data derived by averaging the 8-day data. Then we calculated the anomaly of all maize pixels in different months to assess the seasonal and spatial variations of maize growth during the main growing season from June to September.

2.3.3. Quantifying the impact of typhoon impacts on maize yield

We employed the generalized additive model (GAM) to investigate the association between maize yield and typhoon impacts. The analysis was implemented using the "mgcv" package in R. The GAM is a general method to deal with the nonlinear relationship between the response variable and independent indicators (Hastle and Tibshirani, 1986; Hu et al., 2021). It can balance flexibility and interpretability, and it readily contributes to each independent variable of the maize yield. Specifically,

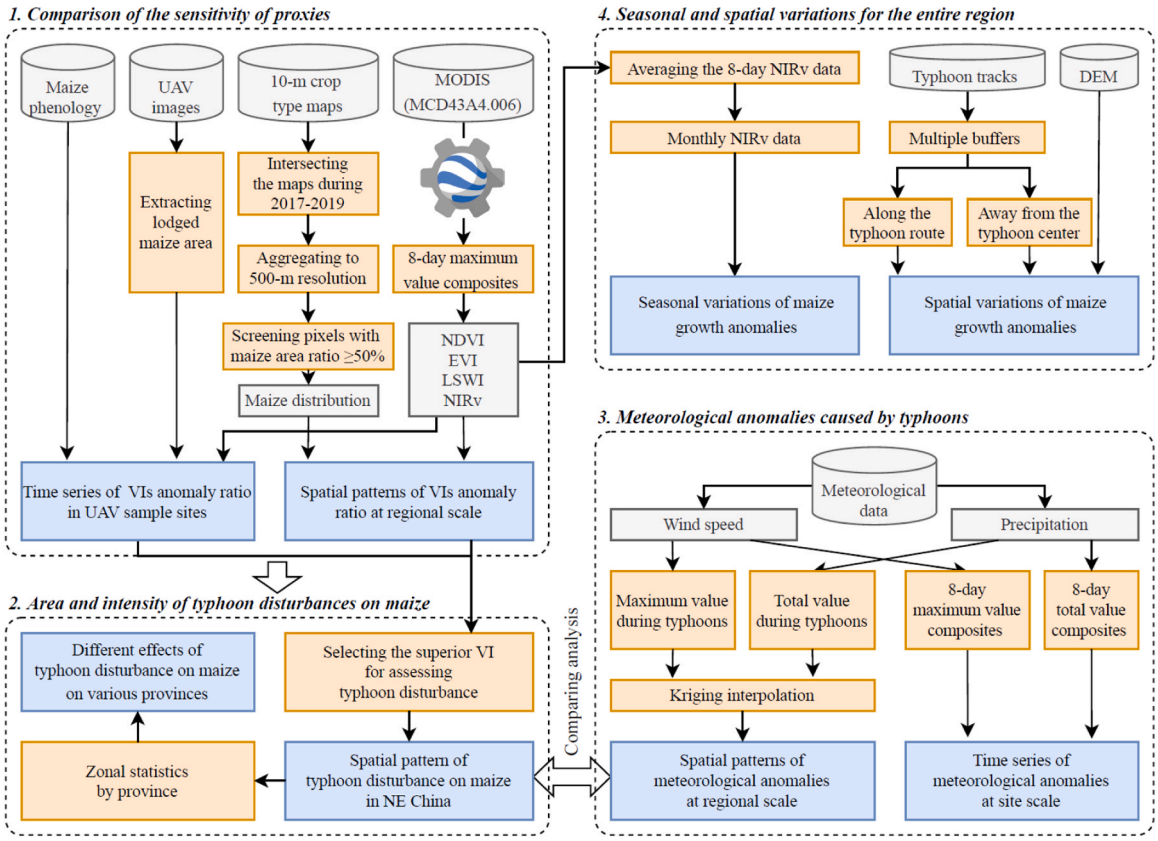

Fig. 4. The framework for rapidly assessing the overall impacts of the typhoon on maize.

we used GAM incorporating cubic regression smoothing spline to model the nonlinear effects of typhoon impacts on maize yield. The constructed model is as follows:

$$\Delta\mathrm{Yield}(\%) = \mathrm{s}\left(\Delta\mathrm{LSWI}_{\mathrm{Before}}(\%)\right) + \mathrm{s}\left(\Delta\mathrm{LSWI}_{\mathrm{After}}(\%)\right) \quad (7)$$

where ΔYield (%) is the relative change of maize yield in 2020. $\Delta\mathrm{LSWI}_{\mathrm{Before}}$ (%) is the relative change of LSWI before the typhoons (May 11 to August 26), representing the state of maize growth before the typhoons in 2020. $\Delta\mathrm{LSWI}_{\mathrm{After}}$ (%) is the relative change of LSWI after the typhoons (September 9 to October 10), representing the state of maize growth after the typhoons in 2020. The *s* donates the cubic smoothing spline function. The Akaike's Information Criterion (AIC) value and R^2 were used as a guide for the goodness of fit of the model.

3. Results

3.1. Sensitivity of the four VIs to detect the impact of typhoon impacts on maize

We analyzed the sensitivity of the four VIs in detecting typhoon impacts on maize at the five UAV sample sites. In site-1, during the typhoon period, the maximum wind speed appeared on DOY 244 in 2020 and reached 13.5 m/s (5.4 m/s higher than the baseline, Fig. 5a), consistent with an increase in precipitation on the same day (107.1 mm in 2020 and 88.3 mm higher than the multiyear means from 2017–2019, Fig. 5b). We found that all the four VIs (LSWI, NDVI, $\mathrm{NIR_V}$, and EVI) began to decrease during the first 8-d after the typhoons (Fig. 5c–f). These decreases continued to enhance until the end of the growing season, with the most significant reductions happening at the end of September (Fig. 5c–f). Among these four indicators, LSWI showed a higher relative change (-161.5%) than $\mathrm{NIR_V}$ (-31.7%), NDVI (-19.7%), and EVI (-25.2%), as shown in Fig. 5, which indicated that LSWI has the highest sensitivity for detecting the typhoon impacts on maize. The results from the other four UAV sites also show consistent conclusions (Figs. S2–5).

Regional-scale analyses also indicated a higher sensitivity of LSWI than others. Fig. 6 shows that LSWI experienced a much larger decrease than $\mathrm{NIR_V}$, NDVI, and EVI after the typhoons. At the beginning of the typhoons (240–247d), there was no obvious difference in the decline of the VIs values. Specifically, LSWI showed an 8.4% reduction (Fig. 6a,e), and $\mathrm{NIR_V}$, NDVI, and EVI values reduced by 5.8% (Fig. 6b,f), 2.2% (Fig. 6c,g), 4.5% (Fig. 6d,h), respectively. The advantages of LSWI in detecting the impact of typhoons on maize growth gradually appeared after the typhoons. LSWI values declined by 69.1% (Fig. 6a,e) at the end of September (272–279d), which is a much more significant decrease than $\mathrm{NIR_V}$ (24.5%, Fig. 6b,f), NDVI (16.5%, Fig. 6c,g), and EVI values (20.4%, Fig. 6d,h).

Although these VIs had different sensitivities for detecting the impacts of typhoons on maize growth, the area of disturbance identified by different proxies was similar. It was about 39.1% (LSWI), 37.9% ($\mathrm{NIR_V}$), 31.2% (NDVI), and 34.0% (EVI) of the maize regions at the beginning (DOY 240), and 72.1%, 75.6%, 70.0%, and 75.1% of the maize regions at the peak (DOY 272) of disturbances (Fig. 7), indicating the agreement among their estimates.

3.2. Area and intensity of typhoon impacts on maize in Northeast China

Given the higher sensitivity of LSWI mentioned above, we used it to examine the area and intensity (i.e., moderate, severe, and extreme impacts) of typhoon impacts on maize in the study area (Fig. 8). During 2017–2019, the mean LSWI values were above zero in most regions of the study area, especially in Heilongjiang and Jilin, even reaching above 0.4 (Fig. 8a), while a significant decline in LSWI values happened in these two provinces after the typhoons in 2020 (Fig. 8b). Specifically, for the entire study area, 15% (2.4 million ha) of the maize area was shown

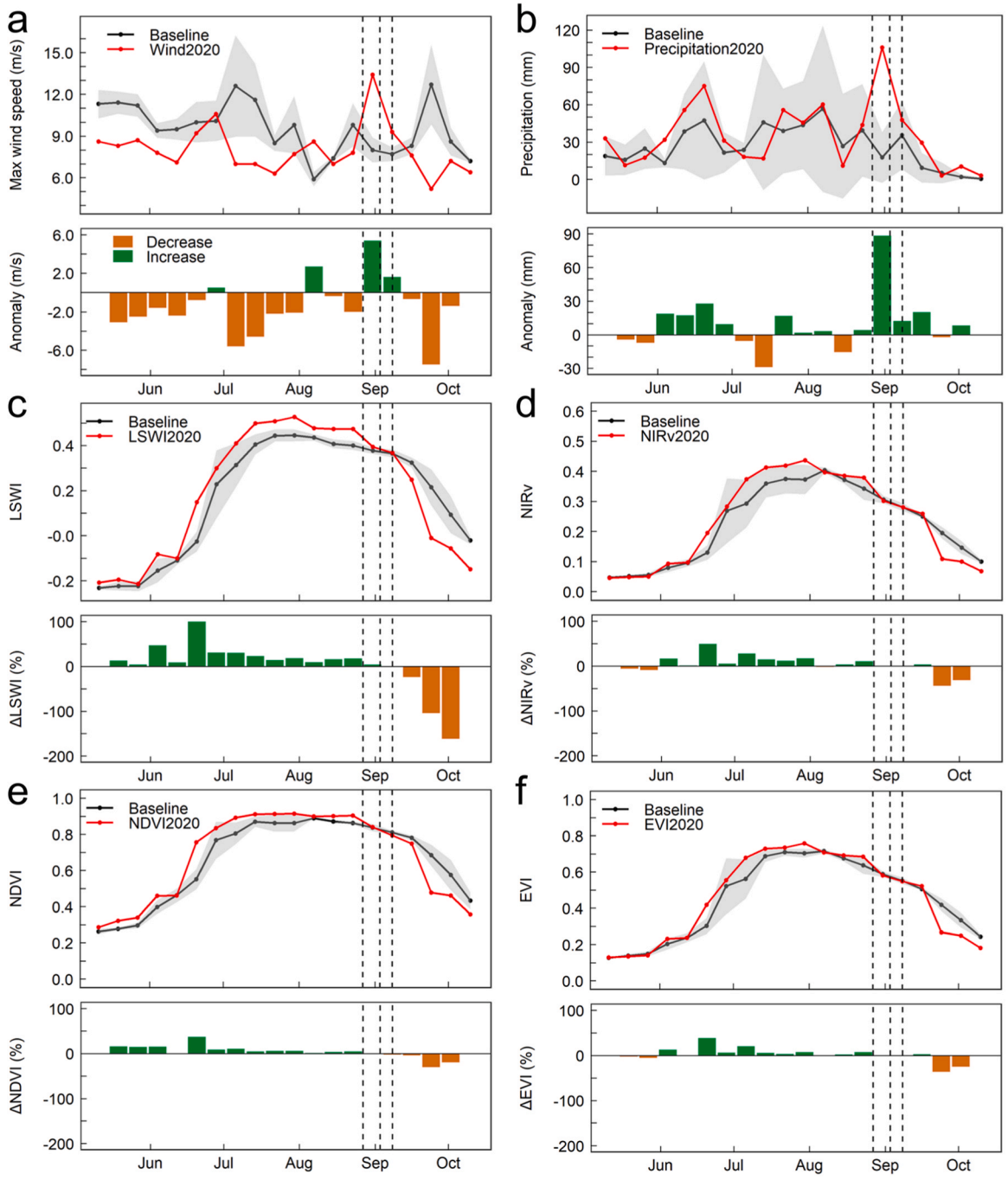

Fig. 5. The meteorological anomalies and the relative change of VIs (ΔVIs (%)) of the UAV sample site-1 during the maize growing season. (a,b) Temporal variations of the 8-day maximum wind speed (a) and total precipitation (b) in 2020 and baseline (2017–2019) and their anomalies. (c–f) Temporal variations of the 8-day LSWI (c), NIR_V (d), NDVI (e), and EVI (f) in 2020 and baseline (2017–2019) and their relative changes, respectively. The coordinates of the weather station and the UAV sample plot center are 126.340555° E, 45.568566° N, and 126.643937° E, 45.425799° N, respectively. The three vertical dashed lines indicate the entry time of the three typhoons (DOY 240, DOY 247, and DOY 252) respectively. The shade of light grey is the range in ± 1 standard deviation in baseline (2017–2019).

as moderate impacts (< −0.5σ) as indicated by LSWI, 16% (2.4 million ha) as severe impacts (< −1.0σ), and 41% (6.7 million ha) as extreme impacts (< −1.5σ) (Fig. 8d).

The typhoon impacts on maize varied in different provinces. Approximately 74% (4.2 million ha, Fig. 9a) and 83% (4.4 million ha, Fig. 9b) of the maize area suffered from typhoon impacts in the Heilongjiang and Jilin, respectively, which were much more than Liaoning (60%, 1.9 million ha, Fig. 9c) and eastern Inner Mongolia (56%, 1.1 million ha, Fig. 9d). Meanwhile, the typhoon impacts in Heilongjiang and Jilin were stronger. Approximately 49% (2.7 million ha, Fig. 9a) and 53% (2.8 million ha, Fig. 9b) of the maize areas in the Heilongjiang and Jilin respectively are affected by extreme impacts (< −1.5σ), while only 25% (0.8 million ha, Fig. 9c) and 15% (0.3 million ha, Fig. 9d) of that in Liaoning and eastern Inner Mongolia respectively.

We also considered the meteorological anomaly of maximum wind speed and total precipitation during the period of the three typhoons (Bavi, Maysak, and Haishen from August 27th to September 8th) to determine the typhoon impacts on the maize area (Fig. 10). The distribution of typhoon impacts on maize area was consistent and located in the estimates from the meteorological anomaly. For example, according

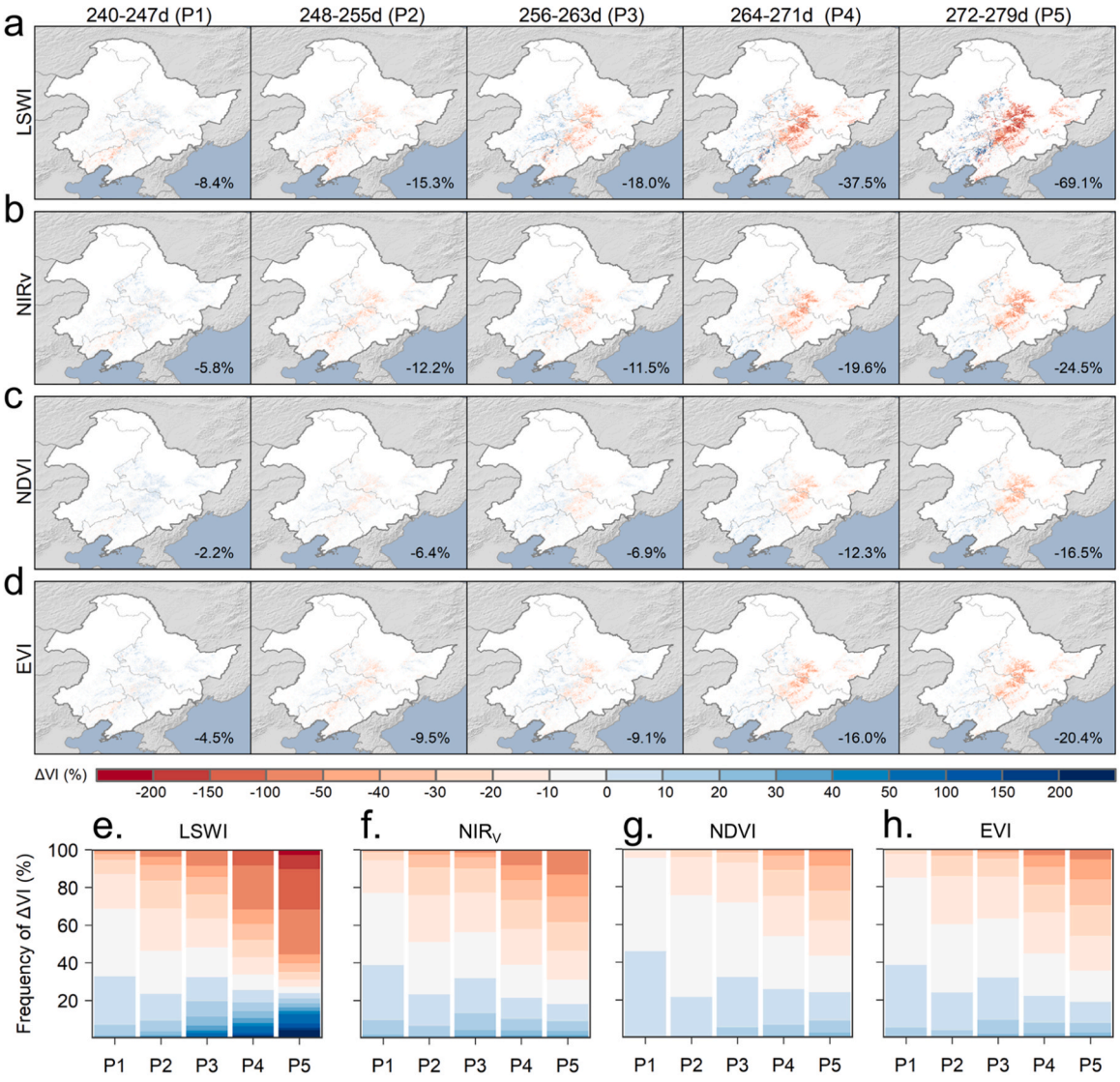

Fig. 6. Spatiotemporal patterns of ΔVIs (%) in 2020 compared to the baseline value during 2017–2019. (a–d) Relative change of LSWI (a), NIR_V (b), NDVI (c), and EVI (d) from Typhoon Bavi to the end of the maize growth period. Numbers beneath each figure show the mean change percent for all pixels with reduced VI value. (e–h) Frequency of different gradients of LSWI (e), NIR_V (f), NDVI (g), and EVI (h) in the corresponding periods.

to the meteorological anomaly, 42% (indicated by maximum wind speed, Fig. 10d) –81% (characterized by total precipitation, Fig. 10h) of the maize area suffered from extreme typhoon impacts, and a total of approximately 62%–85% (Fig. 10d,h) of the regions suffered from typhoon impacts. The areas of LSWI-based typhoon disturbance intensity levels were in the ranges of that according to the meteorological anomaly (Figs. 8 and 10).

3.3. Seasonal and spatial patterns of typhoon impacts on maize growth

We used NIR_V, which is highly correlated with crop biomass accumulation, to examine the seasonal and spatial patterns of maize growth in 2020. Despite suffering from the strong typhoon impacts, we did not find significant reductions in maize growth across the whole study region in 2020 compared to that in the baseline years (2017–2019) (Fig. 11). NIR_V was better than the baseline years from June to August in more than 40% of the study area (mainly in the central region), while approximately 50% of the study area (also in the central region) suffered maize damage in September (Fig. 12). This suggested that maize growth in the previous period (June to August) was generally better than the baseline years, and even though it declined after the typhoons (September), it was the same as the baseline years. We also found that the regions severely affected by typhoons are mainly concentrated in the central regions of Northeast China, while the eastern, western, and northern areas are unaffected or minimally affected by the typhoons (Fig. 12). This suggested a spatial-temporal compensation effect: the better maize growth in the east, west, and northwest of the study area compensates for the poorer maize growth in the central region, and the early stages of maize growth may contribute to increased resilience of maize against subsequent typhoon impacts. The spatial-temporal patterns of the NIR_V anomaly provide additional insights into the overall influence of typhoon impacts on maize (Fig. 12).

3.4. Impacts of typhoon on maize yield

To quantify the impacts of typhoon on maize yield, we employed the ΔLSWI (%) to predict the impacts of typhoon on maize yield and establish the relationship between ΔLSWI (%) and ΔYield (%) utilizing GAM (Fig. 13). The results indicate that the impacts of typhoon can result in a reduction of the maize yield by up to 5% (Fig. 13). This suggests that the impacts of typhoon on maize yield in the region during 2020 was constrained due to their occurrence late in the maize growth

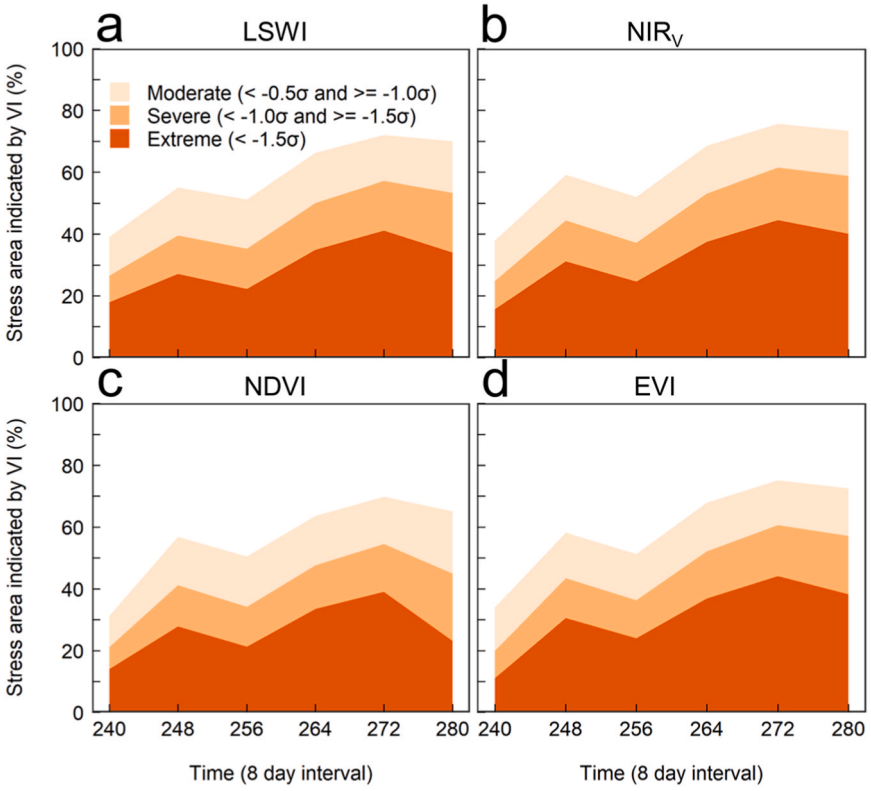

Fig. 7. The 8-day time series of the percentage of the area moderately ($< -0.5\sigma$ and $\geq -1.0\sigma$), severely ($< -1.0\sigma$ and $\geq -1.5\sigma$) and extremely ($< -1.5\sigma$) influenced by the three typhoons. (a–d) The proportion of stress area caused by the three typhoons indicated by LSWI (a), NIR_V (b), NDVI (c), and EVI (d). The σ is the standard deviation in baseline (2017–2019).

cycle, specifically at the milk stage. Regions experiencing higher levels of typhoon impacts exhibited greater yield damage (Fig. 12). The typhoons primarily affected the milk and subsequent physiological maturity stages (Figs. 5 and 6, Table S1), during which starch and nutrient accumulation was nearly complete.

4. Discussion

4.1. Sensitivity of different proxies for assessing typhoon impacts

With the rise in global mean temperatures, the frequency and intensity of EWEs are also increasing (Emanuel, 2005). Crops face heightened vulnerability to the disruptions caused by typhoons, negatively impacting crop yields (Lai, 2017). However, our understanding of the impacts of typhoon on agricultural systems remains limited. Satellite offers the potential to deepen our understanding of maize lodging on a larger spatial-temporal scale. By utilizing satellite data with high temporal and spatial resolutions, readily accessible at no cost, the precise and prompt detection of crop lodging allows for rapid monitoring of maize lodging after typhoons. Satellite-based VIs have been widely employed to monitor the dynamics of land surface and vegetation growth (de Beurs et al., 2019; Gang et al., 2020), but rarely have been focused on the impact of typhoons on crop growth.

In this study, we explored the potential of three greenness indices (NDVI, NIR_V, and EVI) and one water-related index (LSWI) for assessing the impact of typhoons on maize based on high-quality crop maps. Maize lodging results in the complete fracture of maize stems or roots, impeding water absorption and maize growth, typically manifested by a decline in vegetation indices. Our results indicate that LSWI serves as a robust indicator of typhoon impacts on maize in Northeast China (Figs. 5–7). This is because NDVI, NIR_V, and EVI are typically associated with vegetation chlorophyll content (Cheng et al., 2006; Huete et al., 2002). In comparison to changes in leaf chlorophyll content induced by typhoon disturbance, these indices may exhibit delayed and less sensitivity (Zhou et al., 2017). Conversely, water-related vegetation indices, such as LSWI, calculated based on the normalized ratio between NIR and shortwave infrared (SWIR) bands (Xiao et al., 2004), prove to be more sensitive to leaf water content (with a high liquid water absorption rate) and water stress than vegetation greenness-related indices. (Jackson et al., 2004; Wagle et al., 2014). These findings agree with previous studies which found that LSWI, also called Normalized Difference Infrared Index, is a more sensitive indicator of typhoons' or hurricanes' influence on forest ecosystems (Wang et al., 2010). Previous studies also indicated that vegetation dynamics can be better detected by NIR-SWIR-based vegetation indices than the NIR-Red-based ones (Ceccato et al., 2001; Sader et al., 2003).

Some other indices related to vegetation photosynthesis may also be worth considering, such as satellite observations of solar-induced chlorophyll fluorescence (SIF). SIF provides novel measurements to monitor crop growth conditions and stress responses (Porcar-Castell et al., 2014), and many studies have demonstrated that SIF is more sensitive to the photosynthetic rates of plants than other remotely sensed vegetation parameters (Guanter et al., 2014) and it has been widely used in monitoring drought restrictions on vegetation photosynthesis (Song et al., 2018; Wang et al., 2020). However, current SIF products at low spatial resolutions do not seem to be suitable for our study. This problem is expected to be solved with the advent of better spatial and temporal resolution SIF products, which are anticipated from several new satellite instruments such as TROPOMI (Guanter et al., 2015), and the GeoCARB instrument (Rayner et al., 2014).

4.2. Lagging impacts of typhoon impacts on maize

Our investigation revealed that the impact of the typhoon on maize lagged by at least one week and gradually intensified and lasted for a long time until the end of the maize growth season (Fig. 6). Initially, at

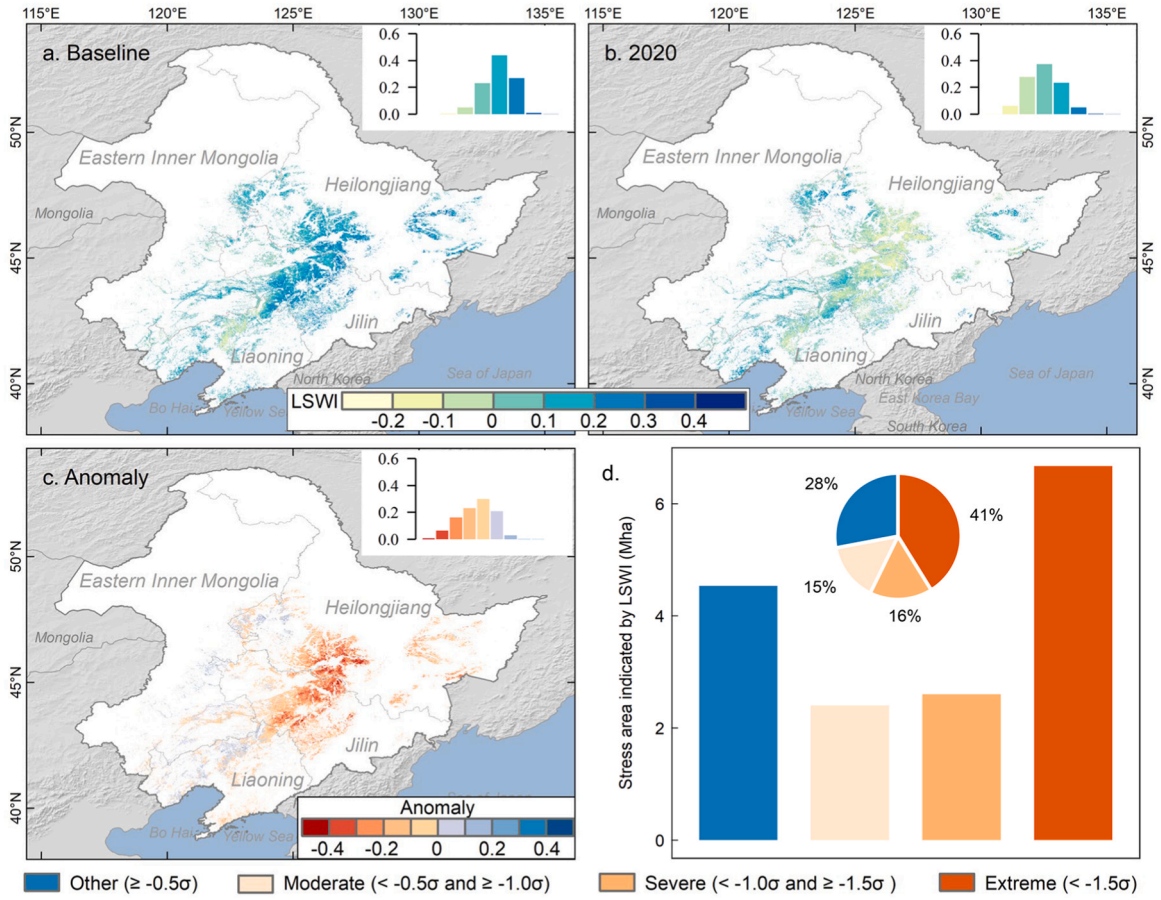

Fig. 8. The area and extent of the typhoon impacts on maize indicated by LSWI in Northeast China in 2020. (a,b) Spatial distributions of LSWI value in Northeast China in baseline (2017–2019) and 2020. The maximum LSWI value at the end of the maize growth period (272–279 days) in 2017–2019 was used as the baseline. (c) Spatial distribution of the LSWI anomaly in Northeast China in 2020. The insets in a–c are the corresponding frequencies. (d) The area moderately ($< -0.5\sigma$ and $\geq -1.0\sigma$), severely ($< -1.0\sigma$ and $\geq -1.5\sigma$), extremely ($< -1.5\sigma$) and other ($\geq -0.5\sigma$) influenced by the three typhoons. The percentage of the four types was shown at the top of the panel.

the onset of the typhoon, around 39% of the maize fields exhibited an 8% decline in LSWI, while towards the end of the maize growth period, approximately 72% of the maize area displayed a substantial 69% decrease in LSWI (Figs. 6a and 7). This lagging impact can likely be attributed to two factors: the delayed response of maize to physiological changes and the time lag in VI responses. On one hand, certain maize plants may not immediately lodge when the typhoons strike, but rather slightly bend initially and then lodge later. This delay could be attributed to the impact of heavy rainfall, which can lead to root failure by weakening the soil strength (Fan et al., 2021), and when combined with strong winds, it increases the self-weight moment of the crop on the stem base (Sylvester-Bradley et al., 1990). Both of these factors significantly elevate the risk of lodging, causing maize plants to lodge after the typhoon, thereby affecting the overall yield (Chauhan et al., 2019). On the other hand, VIs may exhibit lagging responses to the physiological changes in vegetation. Numerous studies have shown that VIs tend to lag by at least approximately 8 days after a shift in precipitation anomaly (Kong et al., 2020; Wang et al., 2003). This delayed response adds to the complexity of assessing the actual impact of the typhoon on vegetation health. The observed lagging impact serves as a warning to continuously monitor crop growth even after typhoon events, as the full extent of the damage may not be immediately evident and could have longer-term implications.

4.3. Spatial-temporal compensations for typhoon impacts on maize

The spatial distribution of typhoon-induced impacts on maize exhibits significant heterogeneity in both spatial patterns and seasonal variations (Figs. 12 and 13), which suggests the spatial-temporal compensation mechanism. On the one hand, maize growth during June, July, and August of 2020 surpassed that of the baseline years (2017–2019) (Figs. 5 and 12). This earlier phase of nutrient accumulation and maturation contributed to bolstering the capacity to withstand the adverse impacts of typhoons in the later stages of the growing season (Ciampitti et al., 2011; Nleya et al., 2016). Consequently, this compensatory mechanism partially alleviated the decline of maize yields caused by the typhoons. On the other hand, the eastern, western, and inland northwest regions of Northeast China exhibited better maize growth, as indicated by the NIR_V, compensating for the damage inflicted on maize in the central region due to typhoons (Fig. 8). This compensatory effect is attributed to the diminishing impact of typhoons on maize as it moves further inland (Chambers et al., 2007), and as the distance from the center of the typhoon route increases (Ayala-Silva and Twumasi, 2004; Zhang et al., 2013).

The spatial heterogeneity in the relative change in maize yield was also consistent with the spatial compensation for the impact of typhoons on maize (Fig. 14 and Fig. S6). According to the statistics, the areas with significant decreases in maize yield were mainly concentrated in the central part of Northeast China in 2020, including Liaoyuan, Siping, Changchun, Daqing, Songyuan, and Baicheng City (Fig. 14 and Fig. S7). Maize yield in other regions of Northeast China was largely unaffected and even much higher than the baseline years. It should be noted that some unaffected regions also suffered from the lower yield including southern Liaoning and Hunlenbuir city (Fig. 14 and Fig. S7), possibly

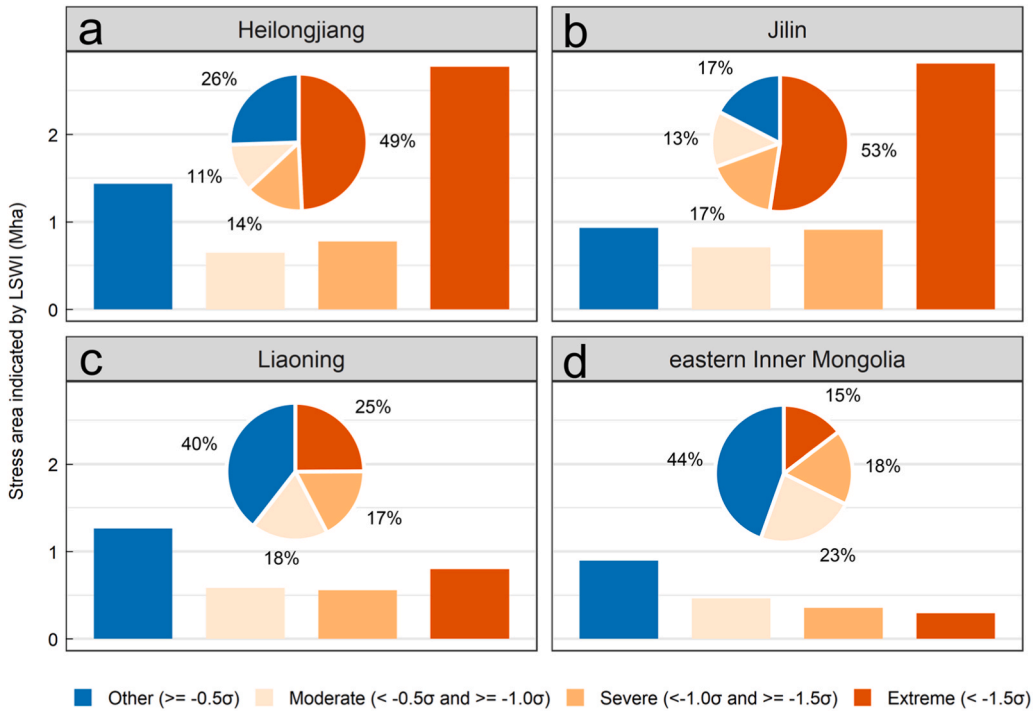

Fig. 9. The difference in typhoon impacts on maize indicated by LSWI on various provinces in Northeast China during the three typhoons (240–252 days) in 2020. (a–d) The area moderately ($< -0.5\sigma$ and $\geq -1.0\sigma$), severely ($< -1.0\sigma$ and $\geq -1.5\sigma$), extremely ($< -1.5\sigma$), and other ($\geq -0.5\sigma$) influenced by the three typhoons in (a) Heilongjiang, (b) Jilin, (c) Liaoning, and (d) eastern Inner Mongolia. The percentage of the four types was shown at the top of each panel.

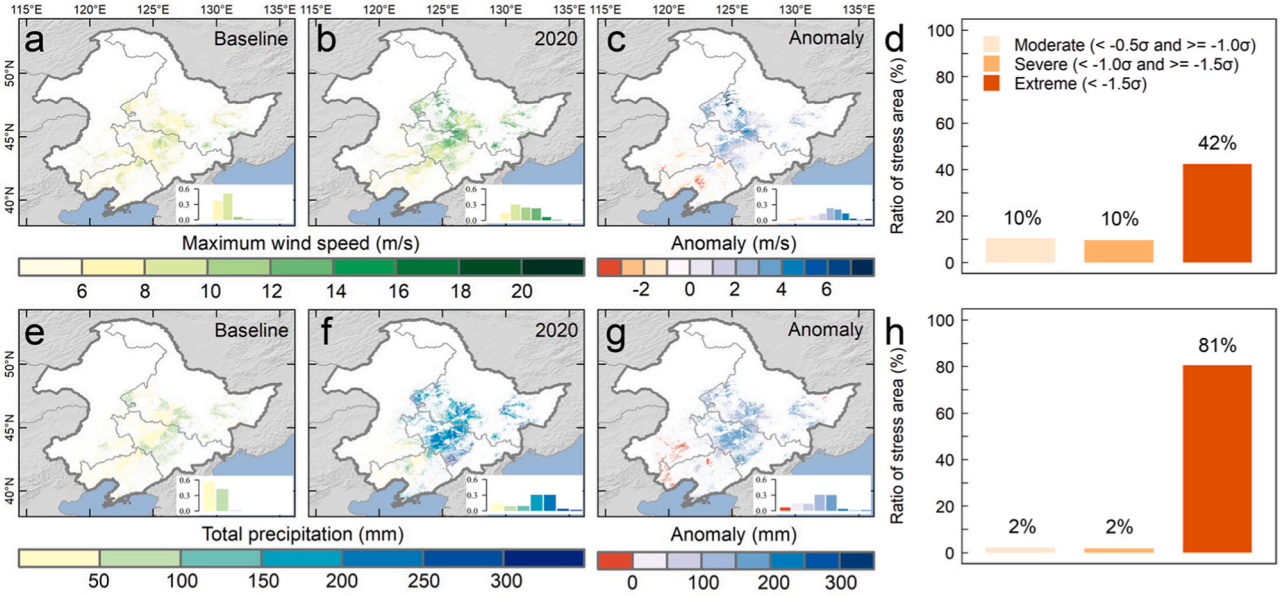

Fig. 10. Spatial patterns of meteorological anomaly in Northeast China during the three typhoons (240–252 days) in 2020. (a,b) Maximum wind speed in baseline (2017–2019) and 2020, respectively. (c) Anomaly of maximum wind speed during the three typhoons. (d) The frequency of the maize area is affected by the maximum wind speed. (e,f) Total precipitation in baseline (2017–2019) and 2020, respectively. (g) Anomaly of total precipitation during the three typhoons. (h) The frequency of the maize area is affected by the total precipitation. The insets in a–c and e–f are the corresponding frequencies.

because the potential flooding could have caused damage to yield there (Mirza, 2011). Several other factors may also influence maize yield. Maize varieties resistant to lodging have enhanced stem diameter coefficients and increased basal internode shattering strength, improving their resilience against strong winds and mitigating potential yield losses (Tong et al., 2020). Additionally, lowering stem density mitigates resource competition, particularly for sunlight, and decreases the likelihood of lodging. (Van Roekel and Coulter, 2011). Rotary tillage enhances lodging resistance by lowering the center of gravity and reinforcing root anchoring strength (Bian et al., 2016).

Despite the impact of typhoons on final maize yield exhibit limitations in Northeast China (Fig. 13), persistent precipitation and waterlogged fields following the occurrence of typhoons can result in varying degrees of yield reduction and quality degradation for maize crops. This

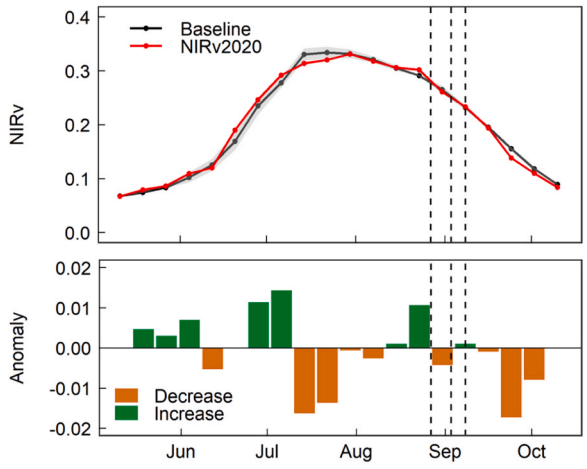

Fig. 11. Temporal variation of NIR_V during the maize growing season in the whole of Northeast China. The upper panel shows the temporal variations of the 8-day NIR_V in 2020 and baseline (2017–2019) and the bottom panel shows the NIR_V anomaly. The three vertical dashed lines indicate the entry time of the three typhoons respectively. The shade of light grey is the range in ± 1 standard deviation in baseline (2017–2019).

is due to abnormal maize growth, slowed kernel dewatering, the presence of moldy and germinating cobs, and increased challenges in the harvesting process (Niu et al., 2016; Tripathi et al., 2005; Webber et al., 2020). Previous studies have highlighted the negative effects of maize lodging, which can further exacerbate the situation by promoting mold development and adversely affecting corn quality (Lindsey et al., 2021; Rajkumara, 2008; Turner et al., 2021). Consequently, a higher proportion of mold-infested kernels may be present in the harvested maize (Jiao et al., 2014). However, our study did not investigate the potential effects of maize mold due to the lack of post-harvest data on maize kernel mass, which needs to be examined in future studies.

4.4. Uncertainty and implications

Previous research has primarily utilized the difference between pre- and post-typhoon VI images to assess the impact of typhoon events on vegetation disturbances (Abbas et al., 2020; Negrón-Juárez et al., 2014). This approach raises concerns regarding the selection of the post-typhoon image for evaluating vegetation disturbance and distinguishing it from seasonal variations in vegetation. To avoid these problems, we compared the VIs in 2020 with the multi-year average (2017–2019, no EWEs) to determine the extent of typhoon-induced impacts on maize. Nevertheless, it is important to note that the natural fluctuations in maize growth across different years, which result in minor variations in VIs unrelated to typhoon impacts, may introduce potential misinterpretations when quantifying the affected maize area, even when using a relatively conservative threshold ($< -0.5\sigma$). It is crucial to underscore that when employing satellite-based VIs to monitor the impact of typhoons on crops, special attention must be paid to the crop growth stages, as this can significantly influence the efficacy of VIs. In our study, the typhoon occurred during the milk stage of maize

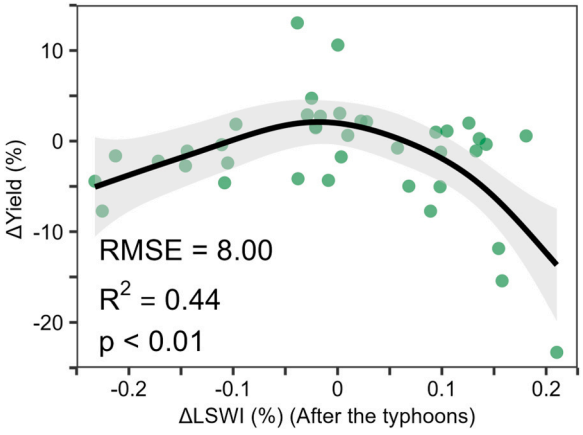

Fig. 13. Contribution of typhoon impacts on maize yield based on GAM.

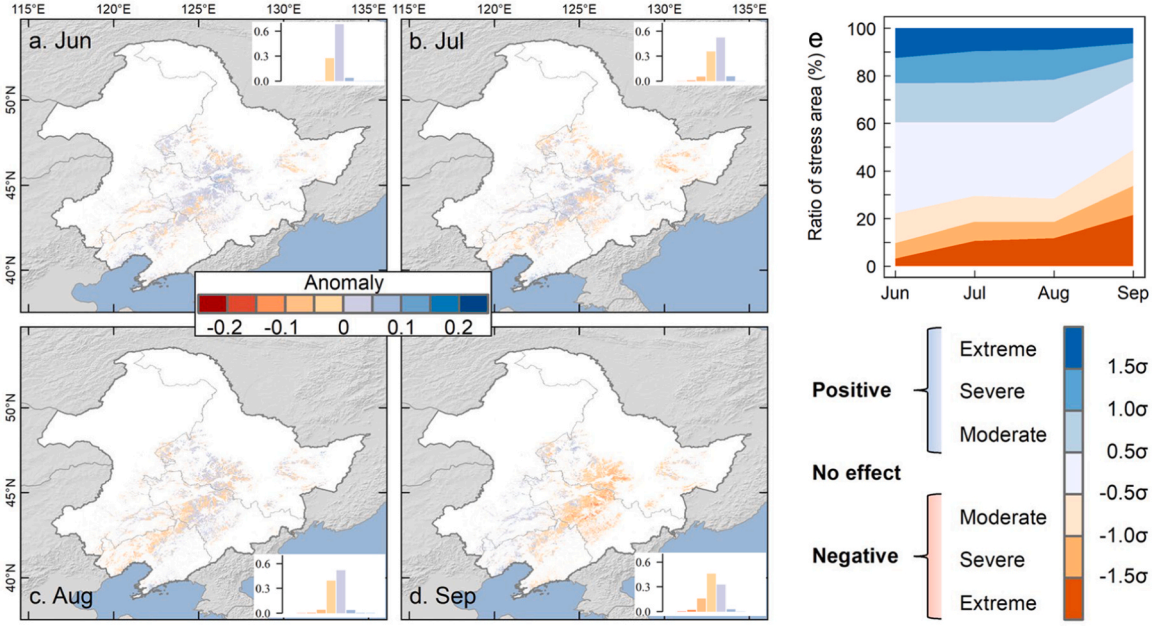

Fig. 12. Spatiotemporal patterns of NIR_V anomaly during maize main growing period. (a–d) Spatial patterns of NIR_V anomaly in (a) June, (b) July, (c) August, and (d) September in 2020 compared to baseline (2017–2019). The insets in a–d are the corresponding frequencies. (e) The monthly time series of the area ratio of different influence gradients.

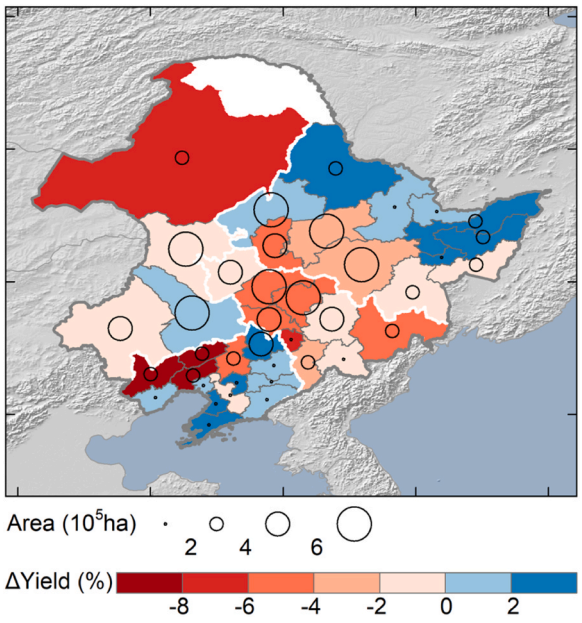

Fig. 14. The planting area and relative change of maize yield in Northeast China in 2020.

when its physical height was nearly at the maturity stage, but nutrient accumulation was still somewhat deficient. Therefore, the lodging caused by the typhoon affects crop nutrient accumulation by influencing processes such as water uptake in maize. If the typhoon occurs when the crops are already fully mature, VIs may struggle to differentiate between lodged and non-lodged crops, requiring further investigation.

The commencement and conclusion of typhoon seasons are generally comprehended, but the occurrence of typhoon events themselves remains unpredictable. Consequently, coordinating ground surveys across the studied landscape becomes challenging due to the uncertainty of disturbances and the location of clouds on satellite images. The collection of ground-truthing data for previous disturbance events was arduous. Therefore, we propose conducting regular ground surveys in multiple frequently affected regions to evaluate the impacts of disturbances on crops whenever feasible. These ground-truthing surveys would enhance the assessment of typhoon impacts on agricultural yields.

5. Conclusions

The impact of three consecutive strong typhoons on maize production in Northeast China has raised concerns about food security amidst the COVID-19 pandemic. Conflicting reports from various agencies and media outlets have further added to public confusion. This study aimed to assess the overall impacts of these typhoons on maize in Northeast China using high-quality maize maps and satellite-based VIs. The analysis revealed that LSWI was more effective than other chlorophyll-related proxies (such as NDVI, NIR_V, and EVI) in monitoring the effects of typhoons on maize growth. The LSWI showed a significantly higher negative relative change of 161.5%, surpassing the corresponding values of 19.7% for NDVI, 31.7% for NIR_V, and 25.2% for EVI. Based on the LSWI results, it was found that a considerable maize field (11.5 million ha) had been affected to varying degrees, with Jilin (4.4 million ha) to Heilongjiang (4.2 million ha), Liaoning (1.9 million ha), and eastern Inner Mongolia (1.1 million ha). The impact of typhoons on maize growth exhibited a delayed response, persisting for a long time until the conclusion of the maize growing season. Interestingly, there was no noticeable decrease in maize growth for the entire Northeast China after the 2020 typhoons compared to the baseline years (2017–2019), which could be attributed to spatial-temporal compensations. This study provided valuable knowledge and a framework for rapid assessment of typhoon impacts by using optimal remote sensing indicators, including the identification of affected areas and patterns, as well as potential impacts on maize production.

CRediT authorship contribution statement

Qiang Zhang: Writing – review & editing, Writing – original draft, Visualization, Validation, Software, Methodology, Investigation, Formal analysis, Data curation, Conceptualization. **Geli Zhang:** Writing – review & editing, Supervision, Resources, Project administration, Investigation, Funding acquisition, Conceptualization. **Nanshan You:** Writing – review & editing, Investigation, Formal analysis. **Yuanyuan Di:** Writing – review & editing, Methodology, Investigation. **Xiangming Xiao:** Writing – review & editing, Investigation. **Yao Zhang:** Writing – review & editing, Supervision, Investigation. **Jinwei Dong:** Writing – review & editing, Supervision, Resources, Project administration, Investigation, Funding acquisition, Conceptualization. **Tong Yang:** Writing – review & editing, Methodology, Investigation. **Yingli He:** Writing – review & editing, Investigation, Data curation.

Declaration of Competing Interest

The authors declare that they have no known competing financial interests or personal relationships that could have appeared to influence the work reported in this paper.

Data availability

The MCD43A4 collection 6 datasets can be obtained from https://lpdaac.usgs.gov/products/mcd43a4v006/. The maize layer is available at https://doi.org/10.1038/s41597-021-00827-9. Tropical cyclone data is available at http://typhoon.nmc.cn/web.html. All the relevant codes from this study could be made available upon request.

Acknowledgments

This work was supported by the Strategic Priority Research Program of the Chinese Academy of Sciences (XDA28060100), the National Natural Science Foundation of China (42271375, 72221002), the Youth Interdisciplinary Team Project of the Chinese Academy of Sciences (JCTD-2021-04), the 2115 Talent Development Program of China Agricultural University, and the funding project of Northeast Geological S&T Innovation Center Zone of China Geological Survey (QCJJ2022-9).

Appendix A. Supporting information

Supplementary data associated with this article can be found in the online version at doi:10.1016/j.eja.2024.127169.

References

Abbas, S., Nichol, J.E., Fischer, G.A., Wong, M.S., Irteza, S.M., 2020. Impact assessment of a super-typhoon on Hong Kong's secondary vegetation and recommendations for restoration of resilience in the forest succession. Agric. For. Meteorol. 280, 107784 https://doi.org/10.1016/j.agrformet.2019.107784.

Abendroth, L.J., Elmore, R.W., Boyer, M.J., Marlay, S.K., 2011. Corn growth and development. Iowa State University Ames.

Anderson, M.C., Neale, C.M.U., Li, F., Norman, J.M., Kustas, W.P., Jayanthi, H., Chavez, J., 2004. Upscaling ground observations of vegetation water content, canopy height, and leaf area index during SMEX02 using aircraft and Landsat imagery. Remote Sens. Environ. 92 (4), 447–464. https://doi.org/10.1016/j.rse.2004.03.019.

Ayala-Silva, T., Twumasi, Y.A., 2004. Hurricane Georges and vegetation change in Puerto Rico using AVHRR satellite data. Int. J. Remote Sens. 25 (9), 1629–1640. https://doi.org/10.1080/01431160310001595037.

Badgley, G., Field, C.B., Berry, J.A., 2017. Canopy near-infrared reflectance and terrestrial photosynthesis. Sci. Adv. 3 (3), e1602244.

Badgley, G., Anderegg, L.D.L., Berry, J.A., Field, C.B., 2019. Terrestrial gross primary production: using NIRv to scale from site to globe. Glob. Chang Biol. 25 (11), 3731–3740. https://doi.org/10.1111/gcb.14729.
Berry, P.M., Sterling, M., Spink, J.H., Baker, C.J., Sylvester-Bradley, R., Mooney, S.J., Tams, A.R., Ennos, A.R., 2004. Understanding and Reducing Lodging in Cereals. Advances in Agronomy. Academic Press, pp. 217–271.
de Beurs, K.M., McThompson, N.S., Owsley, B.C., Henebry, G.M., 2019. Hurricane damage detection on four major Caribbean islands. Remote Sens. Environ. 229, 1–13. https://doi.org/10.1016/j.rse.2019.04.028.
Bian, D.H., Jia, G.P., Cai, L.J., Ma, Z.Y., Eneji, A.E., Cui, Y.H., 2016. Effects of tillage practices on root characteristics and root lodging resistance of maize. FIELD CROPS Res. 185, 89–96. https://doi.org/10.1016/j.fcr.2015.10.008.
Ceccato, P., Flasse, S., Tarantola, S., Jacquemoud, S., Grégoire, J.-M., 2001. Detecting vegetation leaf water content using reflectance in the optical domain. Remote Sens. Environ. 77 (1), 22–33. https://doi.org/10.1016/S0034-4257(01)00191-2.
Chambers, J.Q., Fisher, J.I., Zeng, H., Chapman, E.L., Baker, D.B., Hurtt, G.C., 2007. Hurricane Katrina's carbon footprint on U.S. Gulf Coast forests. Science 318 (5853), 1107. https://doi.org/10.1126/science.1148913.
Chauhan, S., Darvishzadeh, R., Boschetti, M., Pepe, M., Nelson, A., 2019. Remote sensing-based crop lodging assessment: current status and perspectives. ISPRS J. Photogramm. Remote Sens. 151, 124–140. https://doi.org/10.1016/j.isprsjprs.2019.03.005.
Cheng, Y.-B., Zarco-Tejada, P.J., Riaño, D., Rueda, C.A., Ustin, S.L., 2006. Estimating vegetation water content with hyperspectral data for different canopy scenarios: relationships between AVIRIS and MODIS indexes. Remote Sens. Environ. 105 (4), 354–366. https://doi.org/10.1016/j.rse.2006.07.005.
Ciampitti, I.A., Elmore, R.W., Lauer, J., 2011. Corn growth and development. Dent 5 (75), 75.
Elsner, J.B., Kossin, J.P., Jagger, T.H., 2008. The increasing intensity of the strongest tropical cyclones. Nature 455 (7209), 92–95. https://doi.org/10.1038/nature07234.
Emanuel, K., 2005. Increasing destructiveness of tropical cyclones over the past 30 years. Nature 436 (7051), 686–688. https://doi.org/10.1038/nature03906.
Fan, C.-C., Lu, J.Z., Chen, H.H., 2021. The pullout resistance of plant roots in the field at different soil water conditions and root geometries. Catena 207, 105593.
Fischer, R.A., Stapper, M., 1987. Lodging effects on high-yielding crops of irrigated semidwarf wheat. Field Crops Res. 17 (3), 245–258. https://doi.org/10.1016/0378-4290(87)90038-4.
Gang, C., Pan, S., Tian, H., Wang, Z., Xu, R., Bian, Z., Pan, N., Yao, Y., Shi, H., 2020. Satellite observations of forest resilience to hurricanes along the northern Gulf of Mexico. For. Ecol. Manag. 472, 118243 https://doi.org/10.1016/j.foreco.2020.118243.
Guanter, L., Zhang, Y., Jung, M., Joiner, J., Voigt, M., Berry, J.A., Frankenberg, C., Huete, A.R., Zarco-Tejada, P., Lee, J.-E., Moran, M.S., Ponce-Campos, G., Beer, C., Camps-Valls, G., Buchmann, N., Gianelle, D., Klumpp, K., Cescatti, A., Baker, J.M., Griffis, T.J., 2014. Global and time-resolved monitoring of crop photosynthesis with chlorophyll fluorescence. E1327 Proc. Natl. Acad. Sci. 111 (14). https://doi.org/10.1073/pnas.1320008111.
Guanter, L., Aben, I., Tol, P., Krijger, J.M., Hollstein, A., Köhler, P., Damm, A., Joiner, J., Frankenberg, C., Landgraf, J., 2015. Potential of the TROPOspheric monitoring instrument (TROPOMI) onboard the Sentinel-5 Precursor for the monitoring of terrestrial chlorophyll fluorescence. Atmos. Meas. Tech. 8 (3), 1337–1352. https://doi.org/10.5194/amt-8-1337-2015.
Hardisky, M., Klemas, V., Smart, M., 1983. The influence of soil salinity, growth form, and leaf moisture on the spectral radiance of. Spartina Alter. 49, 77–83.
Hastle, T., Tibshirani, R., 1986. Generalized additive models (with discussion). Stat. Sci. 1, 336–337.
Hoque, M.A.-A., Phinn, S., Roelfsema, C., Childs, I., 2016. Assessing tropical cyclone impacts using object-based moderate spatial resolution image analysis: a case study in Bangladesh. Int. J. Remote Sens. 37 (22), 5320–5343.
Hu, S., Xiong, C., Liu, Z., Zhang, L., 2021. Examining spatiotemporal changing patterns of bike-sharing usage during COVID-19 pandemic. J. Transp. Geogr. 91, 102997 https://doi.org/10.1016/j.jtrangeo.2021.102997.
Huete, A., Justice, C., Liu, H., 1994. Development of vegetation and soil indices for MODIS-EOS. Remote Sens. Environ. 49 (3), 224–234. https://doi.org/10.1016/0034-4257(94)90018-3.
Huete, A., Didan, K., Miura, T., Rodriguez, E.P., Gao, X., Ferreira, L.G., 2002. Overview of the radiometric and biophysical performance of the MODIS vegetation indices. Remote Sens. Environ. 83 (1), 195–213. https://doi.org/10.1016/S0034-4257(02)00096-2.
Imbert, D., 2018. Hurricane disturbance and forest dynamics in east Caribbean mangroves. Ecosphere 9 (7), e02231. https://doi.org/10.1002/ecs2.2231.
Jackson, T.J., Chen, D., Cosh, M., Li, F., Anderson, M., Walthall, C., Doriaswamy, P., Hunt, E.R., 2004. Vegetation water content mapping using Landsat data derived normalized difference water index for corn and soybeans. Remote Sens. Environ. 92 (4), 475–482. https://doi.org/10.1016/j.rse.2003.10.021.
Jiao, J., Wang, L., Wang, L., Xiang, H., Jiang, L., 2014. Causes and prevention measures to moldy grain of Maize in Heilongjiang Province. Chin. Agric. Sci. Bull. 30 (30), 228–233.
Jing, Y., Li, J., Weng, Y., Wang, J., 2014. The assessment of drought relief by typhoon Saomai based on MODIS remote sensing data in Shanghai, China. Nat. Hazards 71 (2), 1215–1225.
Kong, D., Miao, C., Wu, J., Zheng, H., Wu, S., 2020. Time lag of vegetation growth on the Loess Plateau in response to climate factors: estimation, distribution, and influence. Sci. Total Environ. 744, 140726 https://doi.org/10.1016/j.scitotenv.2020.140726.
Kossin, J.P., Emanuel, K.A., Vecchi, G.A., 2014. The poleward migration of the location of tropical cyclone maximum intensity. Nature 509 (7500), 349–352.
Kupfer, J.A., Myers, A.T., McLane, S.E., Melton, G.N., 2008. Patterns of Forest Damage in a Southern Mississippi Landscape Caused by Hurricane Katrina. Ecosystems 11 (1), 45–60. https://doi.org/10.1007/s10021-007-9106-z.
Lai, L.-W., 2017. The relationship between extreme weather events and crop losses in central Taiwan. Theor. Appl. Climatol. 134 (1-2), 107–119. https://doi.org/10.1007/s00704-017-2261-z.
Lesk, C., Rowhani, P., Ramankutty, N., 2016. Influence of extreme weather disasters on global crop production. Nature 529 (7584), 84–87. https://doi.org/10.1038/nature16467.
Li, Z., Huang, C., Zhu, Z., Gao, F., Tang, H., Xin, X., Ding, L., Shen, B., Liu, J., Chen, B., Wang, X., Yan, R., 2018. Mapping daily leaf area index at 30 m resolution over a meadow steppe area by fusing Landsat, Sentinel-2A and MODIS data. Int. J. Remote Sens. 39 (23), 9025–9053. https://doi.org/10.1080/01431161.2018.1504342.
Lindsey, A.J., Carter, P.R., Thomison, P.R., 2021. Impact of imposed root lodging on corn growth and yield. Agron. J. 113 (6), 5054–5062. https://doi.org/10.1002/agj2.20848.
Ma, N.L., Peng, W., Soon, C.F., Hassim, M.F.N., Misbah, S., Rahmat, Z., Yong, W.T.L., Sonne, C., 2021. Covid-19 pandemic in the lens of food safety and security. Environ. Res. 193, 110405.
Mirza, M.M.Q., 2011. Climate change, flooding in South Asia and implications. Reg. Environ. Change 11 (1), 95–107. https://doi.org/10.1007/s10113-010-0184-7.
Needham, H.F., Keim, B.D., Sathiaraj, D., 2015. A review of tropical cyclone-generated storm surges: global data sources, observations, and impacts. Rev. Geophys. 53 (2), 545–591.
Negrón-Juárez, R., Baker, D.B., Chambers, J.Q., Hurtt, G.C., Goosem, S., 2014. Multi-scale sensitivity of Landsat and MODIS to forest disturbance associated with tropical cyclones. Remote Sens. Environ. 140, 679–689. https://doi.org/10.1016/j.rse.2013.09.028.
Niu, L., Feng, S., Ding, W., Li, G., 2016. Influence of speed and rainfall on large-scale wheat lodging from 2007 to 2014 in China. PLOS ONE 11 (7), e0157677. https://doi.org/10.1371/journal.pone.0157677.
Nleya, T., Chungu, C., Kleinjan, J., 2016. Corn growth and development. Grow. Corn. Best. Manag. Pract.
Patrick, C.J., Kominoski, J.S., McDowell, W.H., Branoff, B., Lagomasino, D., Leon, M., Hensel, E., Hensel, M.J., Strickland, B.A., Aide, T.M., 2022. A general pattern of trade-offs between ecosystem resistance and resilience to tropical cyclones. Sci. Adv. 8 (9), eabl9155.
Peereman, J., Hogan, J.A., Lin, T.-C., 2020. Assessing typhoon-induced canopy damage using vegetation indices in the Fushan Experimental Forest, Taiwan. Remote Sens. 12 (10), 1654.
Philippopoulos, K., Deligiorgi, D., 2012. Application of artificial neural networks for the spatial estimation of wind speed in a coastal region with complex topography. Renew. Energy 38 (1), 75–82. https://doi.org/10.1016/j.renene.2011.07.007.
Porcar-Castell, A., Tyystjärvi, E., Atherton, J., van der Tol, C., Flexas, J., Pfündel, E.E., Moreno, J., Frankenberg, C., Berry, J.A., 2014. Linking chlorophyll a fluorescence to photosynthesis for remote sensing applications: mechanisms and challenges. J. Exp. Bot. 65 (15), 4065–4095. https://doi.org/10.1093/jxb/eru191.
Rajkumara, S., 2008. Lodging in cereals–a review. Agric. Rev. 29 (1), 55–60.
Rayner, P.J., Utembe, S.R., Crowell, S., 2014. Constraining regional greenhouse gas emissions using geostationary concentration measurements: a theoretical study. Atmos. Meas. Tech. 7 (10), 3285–3293. https://doi.org/10.5194/amt-7-3285-2014.
Rossi, E., Rogan, J., Schneider, L., 2013. Mapping forest damage in northern Nicaragua after Hurricane Felix (2007) using MODIS enhanced vegetation index data. GIScience Remote Sens. 50 (4), 385–399. https://doi.org/10.1080/15481603.2013.820066.
Sader, S.A., Bertrand, M., Wilson, E.H., 2003. Satellite change detection of forest harvest patterns on an industrial forest landscape. For. Sci. 49 (3), 341–353. https://doi.org/10.1093/forestscience/49.3.341.
Schaaf, C.B., Gao, F., Strahler, A.H., Lucht, W., Li, X., Tsang, T., Strugnell, N.C., Zhang, X., Jin, Y., Muller, J.-P., Lewis, P., Barnsley, M., Hobson, P., Disney, M., Roberts, G., Dunderdale, M., Doll, C., d'Entremont, R.P., Hu, B., Liang, S., Privette, J. L., Roy, D., 2002. First operational BRDF, albedo nadir reflectance products from MODIS. Remote Sens. Environ. 83 (1), 135–148. https://doi.org/10.1016/S0034-4257(02)00091-3.
Schwartz, N.B., Uriarte, M., DeFries, R., Bedka, K.M., Fernandes, K., Gutiérrez-Vélez, V., Pinedo-Vasquez, M.A., 2017. Fragmentation increases wind disturbance impacts on forest structure and carbon stocks in a western Amazonian landscape. Ecol. Appl. 27 (6), 1901–1915. https://doi.org/10.1002/eap.1576.
Smith, A.M.S., Kolden, C.A., Tinkham, W.T., Talhelm, A.F., Marshall, J.D., Hudak, A.T., Boschetti, L., Falkowski, M.J., Greenberg, J.A., Anderson, J.W., Kliskey, A., Alessa, L., Keefe, R.F., Gosz, J.R., 2014. Remote sensing the vulnerability of vegetation in natural terrestrial ecosystems. Remote Sens. Environ. 154, 322–337. https://doi.org/10.1016/j.rse.2014.03.038.
Smith, N.E., Kooijmans, L.M.J., Koren, G., van Schaik, E., van der Woude, A.M., Wanders, N., Ramonet, M., Xueref-Remy, I., Siebicke, L., Manca, G., Brümmer, C., Baker, I.T., Haynes, K.D., Luijkx, I.T., Peters, W., 2020. Spring enhancement and summer reduction in carbon uptake during the 2018 drought in northwestern Europe. Philos. Trans. R. Soc. B: Biol. Sci. 375 (1810), 20190509 https://doi.org/10.1098/rstb.2019.0509.
Song, L., Guanter, L., Guan, K., You, L., Huete, A., Ju, W., Zhang, Y., 2018. Satellite sun-induced chlorophyll fluorescence detects early response of winter wheat to heat stress in the Indian Indo-Gangetic Plains. Glob. Change Biol. 24 (9), 4023–4037. https://doi.org/10.1111/gcb.14302.
Stanturf, J.A., Goodrick, S.L., Outcalt, K.W., 2007. Disturbance and coastal forests: a strategic approach to forest management in hurricane impact zones. For. Ecol. Manag. 250 (1), 119–135. https://doi.org/10.1016/j.foreco.2007.03.015.

Sylvester-Bradley, R., Scott, R., Wright, C., 1990. Physiology in the production and improvement of cereals. Physiology in the production and improvement of cereals. 18.

Tong, S., Du, Z., Li, C., Song, F., 2020. Comparison of stem characteristics and screening of lodging resistance varieties in Sanjiang Plain. Mol. Plant Breed. 18 (17), 5860–5868.

Tortini, R., van Manen, S., Parkes, B., Carn, S., 2017. The impact of persistent volcanic degassing on vegetation: a case study at Turrialba volcano, Costa Rica. Int. J. Appl. earth Obs. Geoinf. 59, 92–103.

Tripathi, S.C., Sayre, K.D., Kaul, J.N., 2005. Planting systems on lodging behavior, yield components, and yield of irrigated spring bread wheat. Crop Sci. 45 (4), 1448–1455. https://doi.org/10.2135/cropsci2003-714.

Turner, A.P., Jackson, J.J., Sama, M.P., Montross, M.D., 2021. Impact of delayed harvest on corn yield and harvest losses. Appl. Eng. Agric. 37 (4), 595–604. https://doi.org/10.13031/aea.14561.

Van Roekel, R.J., Coulter, J.A., 2011. Agronomic responses of corn to planting date and plant density. Agron. J. 103 (5), 1414–1422. https://doi.org/10.2134/agronj2011.0071.

Wagle, P., Xiao, X., Torn, M.S., Cook, D.R., Matamala, R., Fischer, M.L., Jin, C., Dong, J., Biradar, C., 2014. Sensitivity of vegetation indices and gross primary production of tallgrass prairie to severe drought. Remote Sens. Environ. 152, 1–14. https://doi.org/10.1016/j.rse.2014.05.010.

Wang, F., D'Sa, E.J., 2009. Potential of MODIS EVI in Identifying Hurricane Disturbance to Coastal Vegetation in the Northern Gulf of Mexico. Remote Sens. 2 (1), 1–18. https://doi.org/10.3390/rs2010001.

Wang, F., Xu, Y.J., 2009. Hurricane Katrina-induced forest damage in relation to ecological factors at landscape scale. Environ. Monit. Assess. 156 (1), 491–507.

Wang, J., Rich, P.M., Price, K.P., 2003. Temporal responses of NDVI to precipitation and temperature in the central Great Plains, USA. Int. J. Remote Sens. 24 (11), 2345–2364. https://doi.org/10.1080/01431160210154812.

Wang, M., Xu, H., 2018. Remote sensing-based assessment of vegetation damage by a strong typhoon (Meranti) in Xiamen Island, China. Nat. Hazards 93 (3), 1231–1249. https://doi.org/10.1007/s11069-018-3351-7.

Wang, S., Zhang, Y., Ju, W., Porcar-Castell, A., Ye, S., Zhang, Z., Brümmer, C., Urbaniak, M., Mammarella, I., Juszczak, R., 2020. Warmer spring alleviated the impacts of 2018 European summer heatwave and drought on vegetation photosynthesis. Agric. For. Meteorol. 295, 108195.

Wang, S., Zhang, Y., Ju, W., Qiu, B., Zhang, Z., 2021. Tracking the seasonal and inter-annual variations of global gross primary production during last four decades using satellite near-infrared reflectance data. Sci. Total Environ. 755, 142569 https://doi.org/10.1016/j.scitotenv.2020.142569.

Wang, W., Qu, J.J., Hao, X., Liu, Y., Stanturf, J.A., 2010. Post-hurricane forest damage assessment using satellite remote sensing. Agric. For. Meteorol. 150 (1), 122–132. https://doi.org/10.1016/j.agrformet.2009.09.009.

Webber, H., Lischeid, G., Sommer, M., Finger, R., Nendel, C., Gaiser, T., Ewert, F., 2020. No perfect storm for crop yield failure in Germany. Environ. Res. Lett. 15 (10), 104012 https://doi.org/10.1088/1748-9326/aba2a4.

Wolf, S., Keenan, T.F., Fisher, J.B., Baldocchi, D.D., Desai, A.R., Richardson, A.D., Scott, R.L., Law, B.E., Litvak, M.E., Brunsell, N.A., Peters, W., van der Laan-Luijkx, I. T., 2016. Warm spring reduced carbon cycle impact of the 2012 US summer drought. Proc. Natl. Acad. Sci. 113 (21), 5880–5885. https://doi.org/10.1073/pnas.1519620113.

Wu, G., Guan, K., Jiang, C., Peng, B., Kimm, H., Chen, M., Yang, X., Wang, S., Suyker, A. E., Bernacchi, C.J., 2020. Radiance-based NIRv as a proxy for GPP of corn and soybean. Environ. Res. Lett. 15 (3), 034009.

Xiao, X., Hollinger, D., Aber, J., Goltz, M., Davidson, E.A., Zhang, Q., Moore, B., 2004. Satellite-based modeling of gross primary production in an evergreen needleleaf forest. Remote Sens. Environ. 89 (4), 519–534. https://doi.org/10.1016/j.rse.2003.11.008.

You, N., Dong, J., Huang, J., Du, G., Zhang, G., He, Y., Yang, T., Di, Y., Xiao, X., 2021. The 10-m crop type maps in Northeast China during 2017-2019. Sci. Data 8 (1), 41. https://doi.org/10.1038/s41597-021-00827-9.

Zeng, Z., Ziegler, A.D., Searchinger, T., Yang, L., Chen, A., Ju, K., Piao, S., Li, L.Z.X., Ciais, P., Chen, D., Liu, J., Azorin-Molina, C., Chappell, A., Medvigy, D., Wood, E.F., 2019. A reversal in global terrestrial stilling and its implications for wind energy production. Nat. Clim. Change 9 (12), 979–985. https://doi.org/10.1038/s41558-019-0622-6.

Zhang, X., Wang, Y., Jiang, H., Wang, X., 2013. Remote-sensing assessment of forest damage by Typhoon Saomai and its related factors at landscape scale. Int. J. Remote Sens. 34 (21), 7874–7886. https://doi.org/10.1080/01431161.2013.827344.

Zhou, Y., Xiao, X., Zhang, G., Wagle, P., Bajgain, R., Dong, J., Jin, C., Basara, J.B., Anderson, M.C., Hain, C., 2017. Quantifying agricultural drought in tallgrass prairie region in the US Southern Great Plains through analysis of a water-related vegetation index from MODIS images. Agric. For. Meteorol. 246, 111–122.